ESTIMATION OF UNDERGROUND STRUCTURE AROUND THE SABAE FAULT BASED ON MICROTREMOR OBSERVATION

Proceedings of the International Symposium on Geo-informatics and Zoning for Hazard Mapping, pp. 285-290

ESTIMATION OF UNDERGROUND STRUCTURE AROUND THE SABAE FAULT BASED ON MICROTREMOR OBSERVATION

Keisuke Kojima[1], Hirofumi Yamamoto[2], Tasuya Noguchi[3],
Takuo Okamoto[4], Eiji Nakaya[3] and Koudai Moto[1]

[1]*Graduate School of Engineering, The University of Fukui, Japan*
[2]*Faculty of Education and Regional Studies, The University of Fukui, Japan*
[3]*Graduate School of Engineering, Tottori University, Japan*
[4]*Course of General Education, Fukui National College of Technology, Japan*

ABSTRACT

Reliable Quaternary structure is indispensable in order to accurately predict the seismic damage of the region. We executed microtremor observations along the several exploration lines orthogonal to the Sabae Fault. The phase velocities of surface waves were calculated from the array observations by applying the spatial autocorrelation analysis. The dispersion curves were inverted to a vertical S-wave profile using a genetic algorithm. To interpolate the array observations, the single-point 3-components observations were made. It was confirmed that there were two predominant periods in the H/V spectrum and each predominant period were caused by the Alluvium and the Diluvium respectively. We estimated the Quaternary configuration from these predominant periods using the estimated S-wave velocities based on the quarter wavelength rule. The 3D S-wave structure model was proposed by using the vertical structure of the microtremor observation sites. Furthermore, we observed gravity anomaly and calculate the density structure. The validity of the estimated structure from the microtremor observation was confirmed by comparing with the density structure and with the existing deep well data. The estimated configuration showed that the Quaternary deposit has a folded mound near the Sabae fault and that the lower diluvium is shifting over 100m across the fault.

Keywords: Sabae Fault, microtremor observation, inversion, underground configuration

1 INTRODUCTION

Recently, considerably large earthquakes have continuously occurred around Japan Sea coastal area. In addition, so-called the Niigata-Kobe Tectonic Zone has been pointed out that is a shear strain concentration zone detected from the successive monitoring of the reference points by using the GPS. Besides, by considering the distribution of many active faults in and around Fukui prefecture, we should keep our expectations realistic for the seismicity of this prefecture. The Sabae Fault has been attracting attention among the active faults in Fukui Prefecture. The fault is located on the center of the Fukui Plain lying from the south of Fukui City to Echizen City through the urban area of Sabae City. The Research Group for Active faults of Japan listed the Sabae Fault as the certainty II, the degree of activity B, the strike NS, the western side up heaved and the length is 8km. The Chronological Scientific Tables list two historical earthquakes occurred around the fault; those are the earthquakes in 1639 of M=6 and in 1900 of M=5.8. However, no evidence of fault displacement accompanying the historical earthquakes has been confirmed. Furthermore, a seismic gap around the fault has been pointed out from the microearthquake observation. Yamamoto discovered the Kikai-Akahoya tephra (K-Ah: erupted 7300 years ago) in the Holocene deposits overlaying the Pleistocene gravel layers at the outcrop on the Sabae Plateau. He indicated that the activity and certainty of the Sabae Fault should be revised considering the large offset between the K-Ah layer in the plateau and the one in the east lowland. By considering above mentioned aspects, it can be said that the Sabae Fault is one of the most imperative faults to survey around Fukui Prefecture.

In this study, we discuss the Quaternary configuration across the Sabae Fault based on the microtremor and gravity anomaly observation. Array observations and single-site 3-components observations of microtremor were carried out along the four exploration sections across the fault. We could evaluate two kinds of predominant period in the collected Fourier and H/V spectra of microtremor. It was confirmed that those predominant periods were originated on the basement of alluvium and diluvium respectively. The S-wave structures under the array sites were inverted based on the observed Rayleigh-wave dispersion curves. By integrating those results, the Quaternary configuration across the fault was estimated. To compliment the estimated configuration from the microtremor, we carried out additional gravity exploration around the fault and determined the density structure based on the Bouguer gravity anomaly.

2 SABAE FAULT

2.1 Topography

Figure 1 is a topographic map around the Sabae Fault. The Seibu (Sabae-Takefu) Basin is located on the center of the Reihoku district of Fukui Prefecture; it extends over about 10km in the east-west direction and 13km in the north-south. The Sabae Plateau extends from Mt. Kyoga to

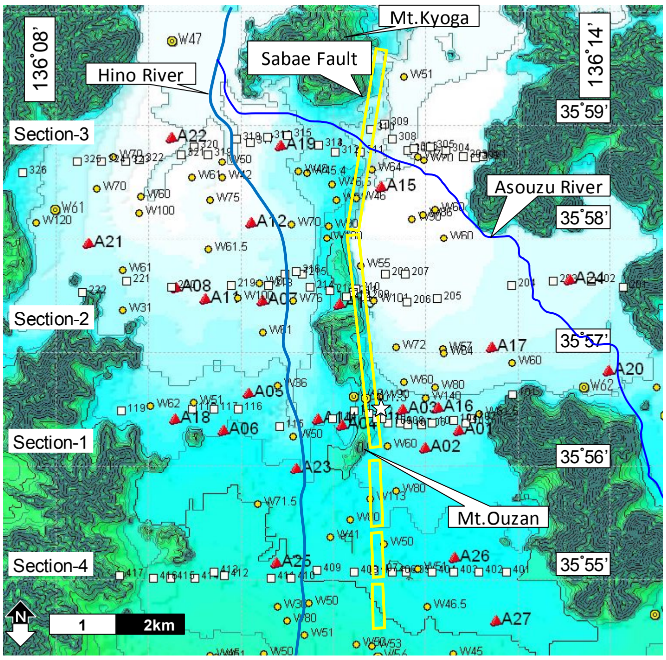

Figure 1. Topography around the Sabae fault and locations of the microtremor observation sites (☆: Trenching point, ▲: Array site, □ : single-point 3-component observation site, ◇ : single-point 3-component observation site (outcrop point), ○ : deep well (not attained to base rock), ◎ : deep well (attained to base rock)

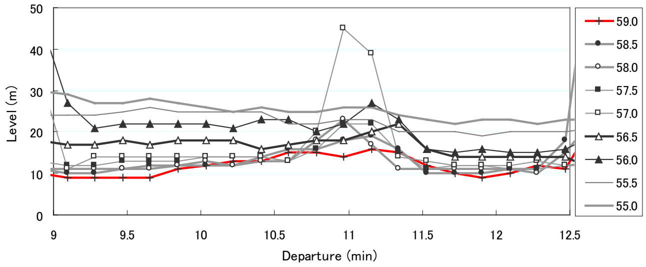

Figure 2. Elevation sections in the east-west direction

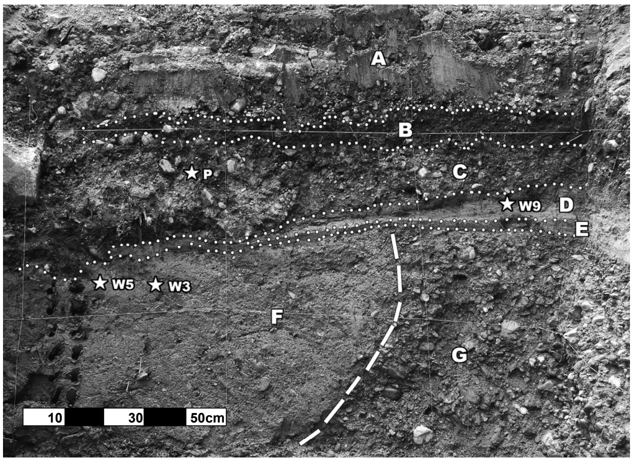

Figure 3. Outcrop of the Sabae Fault on the south-wall in the trench, ☆ shows sampling points for ^{14}C dating

Mt. Ouzan in the center of the basin. The east margin of the plateau is considered corresponding to the Sabae Fault. The Hino River flows along the western lowland in the north-south direction as a mainstream of the Seibu Basin. The western lowland is covered by the flood plain and the alluvial fan deposits originated on this river. The west lowland is mainly covered by the flood plain whereas the east lowland is partially composed by the backswamp deposits. The Mountains surrounding the Basin are mainly consisted of Neogene Andesitic Rocks (the Ito-o Formation) and partially of Cretaceous Rhyolitic Rocks. Figure 2 shows the present topography orthogonal to the Sabae Fault. The symbols in the figure correspond to the elevations along the meridian sections from northern latitude of 35°55' to 36° at intervals of 1 minute. We can point out from this figure that the western side of the Sabae plateau has a gentle slope whereas the eastern side shows steep cliff like configuration and that the western lowland is relatively high than the eastern lowland.

2.2 Trenching Survey

The Sabae Fault was delineated on the basis of the topographic features and the distribution of spring waters. Unfortunately, any outcrop of the fault plane had not found. The authors (2008) conducted a trenching survey at the parking lot of a hospital in front of the JR Sabae station. As shown in Figure 1, the trenching site corresponds approximately to the mid part of the fault. Figure 3 shows the exposed fault plane on the south wall of the trench. The fault separates the gravel layer G continuing from the Sabae Plateau against the silty-clay layer constituting the Sabae east lowland. The Kikai-Akahoya tephra erupted at about 7,300 years ago was detected in the layer F. The radio active carbon dating was executed by using the organic samples (wood pieces and pine cones) obtained from the layers. The three carbonized wood chips from the uppermost part of the layer F showed 2870-2620, 2120-2090, and 2040-1960 B.C., respectively. On the other hand, we got carbon ages of 1420-1440 A.D. by the wood pieces retrieved from the layer D that have not been heaved by the fault. According to those radioactive dating results, it can be said that the fault moved at least one time from 2900 B.C. to 1400 A.D. The concentration of the latest activity age of the fault was not sufficient to calculate the earthquake occurrence rate and predict the next event. Another trenching and boring surveys are planned to elucidate the activity history of the fault.

3 MICROTREMOR OBSERVATION

3.1 Location and condition

Figure 1 shows the microtremor observation sites on the topographical map around the Seibu basin. Four east-west prospecting sections were set almost orthogonal to the Sabae Fault. We arranged microtremor array observation stations and single-point 3-components observation sites along those exploration liens. The closed triangles and the circles in the figure indicate the array observation stations and the single-point observation sites, respectively. The array sites were named as "A" plus a number in the order of observation. The single-point observation sites were termed by 3-digites-numbers. The 1st number means the prospecting section and remaining 2-digits-number represents observation point number counting from the westernmost point.

The array observation system consisted of four transducers and a seismic data recorder. The microtremors were observed by a three components seismometer, JEP6A3, located on the centroid and three vertical seismometers, JEP6A1, placed on vertices of a equilateral triangle. The array observation was executed by using three kinds of

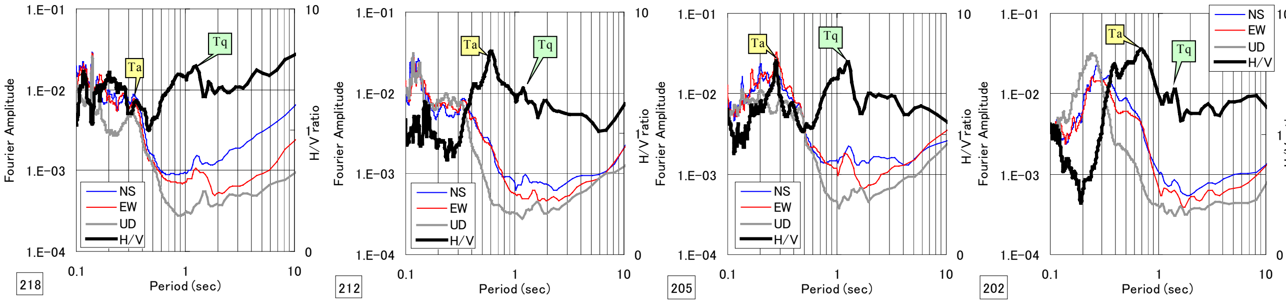

Figure 4. H/V spectra from single-point 3-element microtremor observation (Section-2)

radii within the range from 4m to be 50m for each site according to the situation. At any observation sites, microtremors were recorded simultaneously for about 5minutes and digitized at a sampling frequency of 100Hz. The single point 3-components observations were made with a JEP6A3 type seismometer and the data recorder. The condition of sampling rate and duration is same as the array observation.

3.2 H/V spectrum ratio of microtremor

Five data segments of 40.96s each without significant artificial noise were selected from the observed microtremor data. The Fourier spectra were smoothed by Parzen window with a band width of 0.3Hz. The horizontal-to-vertical spectral ratio (H/V) was calculated by dividing the multiply mean values of NS and EW elements by the vertical element. Figure 4 shows examples of the H/V spectrum ratio of the exploration section 2 by which the trenching survey site is passed. We can find two peaks of H/V spectrum ratio as typically seen at the 205 point. After Nakamura's proposal of the H/V spectral ratio, many studies have confirmed that the predominant period of H/V spectrum corresponds to the natural period of the site. The authors (2004) judged that these peaks were corresponding to the natural periods of the site that originate on the alluvium and the Quaternary stratum from the regression analytical result between the predominant periods observed in the Fukui Plain and the corresponding boring depths. In this study, the shorter predominant period is referred as Ta and the longer one is described as Tq. The subscript "a" represents the alluvium and "q" represents the quaternary formation.

The open circles and the filled circles in Figure 5 show the distribution of Ta and Tq along the exploration lines, respectively. It can be seen that those predominant periods tend to decrease over the Sabae Plateau area. There are some discontinuities of the predominant period just on the both margins of the Sabae Plateau. The gray lines in the figure exhibit the natural periods of the alluvium calculated from the Fukui Prefecture's S-wave velocity Model (F-Model) by using the quarter wavelength rule. The black lines indicate those values of the Quaternary deposits. The F-Model was adopted by Fukui Prefecture for the earthquake disaster prediction survey (1997). Note that the reliability of F-Model is not necessarily high, because the model was estimated from the shallow boring data, a small number of deep wells and the surface geological feature.

3.3 Phase velocity of Rayleigh wave

The dispersion curves of the Rayleigh-wave were calculated by using the spatial autocorrelation method

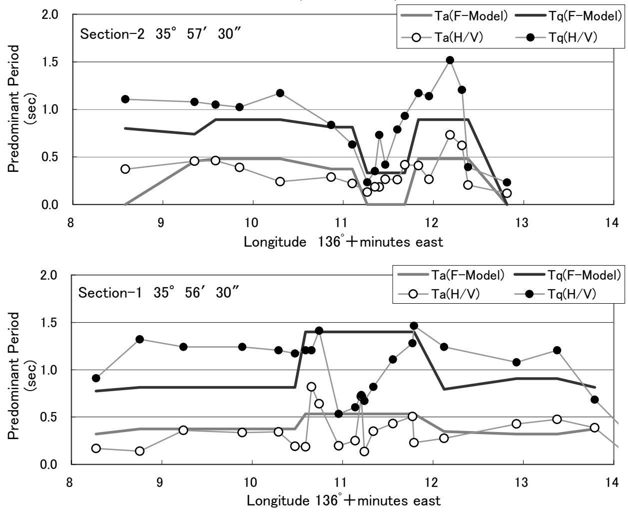

Figure 5. Distribution of predominant periods along exploration lines 1 and 2.

(SPAC) based on the observed vertical microtremor at the array sites. The number of a data segment and the overlapping number were set to 2048 and 512, respectively. Over 15 sets of data segments with 2048 points each were selected from the digitized data. The average and the variance of the phase velocity can be calculated from those data segments.

Figure 6 shows the dispersion curves of the A01 and A04 array sites. The circles and the two thin lines represent the average and the standard deviations of the phase velocity. As shown in Figure 1, the A01 site is located on the east low land covered by the backswamp deposits, on the other hand the A04 site is situated on the Sabae Plateau. The phase velocities of the A01 site show smooth normal dispersibility and they are lower values than those of the A04 site over whole frequency range. These phase velocities seem to be harmonized with the ground conditions of the sites.

4 UNDERGROUND CONFIGURATION

4.1 Inversion

As shown in Figure 6, the dispersion curves of the Rayleigh wave were obtained at each array observation site. In this thesis, the inversion of the S-wave velocity structure of array sites is formulated as an optimization problem based on the observed dispersion curve. To obtain a unique profile stably, the following assumptions were made: (1) densities are treated as known values and are set to typical values for each soil classification. (2) P-wave velocities can be found from S-wave velocities by the next empirical equation (Kitsunezaki et al. 1990):

$Vp = 1.11 \cdot Vs + 1290$ (m/s). Thus this inversion problem is formulated as an optimization problem to modify H and Vs which minimize the following objective function, J. The function is a sum of squares of the differences between the observed dispersion curve and those values calculated for the assumed S-wave velocity structure.

$$J = \sum_{i=1}^{N_f^c} \left(\frac{C_i^O - C_i^C}{\sigma_i^O} \right)^2 \rightarrow \text{minimize} \qquad (1)$$

where C_i^O, C_i^C :observed and calculated phase velocity of i-th frequency, σ_i^O :standard deviation of C_i^O , respectively. It is not easy to solve the formulated optimization problem analytically, because of the high nonlinearity in the objective function. We utilized a genetic algorithm to search the optimal modification rates of thickness and S-wave velocities from the initial values. Since the optimized S-wave structure is supposed to depend on the initial structure, the initial structure should be determined with discretion. We set the initial S-wave velocity structure based on the observed dispersion curve by using the empirical formula proposed by Nagao and Konno (2001), between the Rayleigh-wave phase velocity (C_λ) at the wave length λ and the averaged S-wave velocity ($\overline{Vs}_Z$) from the surface to a depth Z. The reader is referred to Kojima et al (2004) for more details of the procedure. Thick gray lines in Figure 7 are the initial S-wave velocity structure models of the array sites. The initial structure was determined as a four-layers model having two alluvial layers and two diluvial ones. Solid lines in Figure 6 are the theoretical phase velocity computed for the inverted S-wave profiles while gray lines are those calculated for the initial profiles. The computed values show fairly good agreement with the observed ones at both stations. The thick black line in figure 7 shows the identified S-wave profile. It can be seen that the alluvial structures are optimized near the initial ones, however, the diluvial structures are identified away from the initial values. It is worth noting that the optimized S-wave velocities of upper two layers in the array site located on the Sabae Plateau (A04 site) are larger than those of the back swamp (A01).

4.2 Estimation of Quaternary Configuration

Based on the predominant periods of the microtremor H/V spectrum and the inverted S-wave structure, we estimated the quaternary configuration along the exploration lines. The assumptions and the procedure are as follows. (1) the predominant periods of the H/V spectrum, Ta and Tq, are assumed to be the natural site periods for multiple reflected S-waves. (2) the quarter-wavelength rule is available for each observation site. (3) both the alluvium and the diluvium consist of two layers. (4) the values of S-wave velocity for each layer of the single-point 3-components observation site are interpolated from the inverted structures of the array site in vicinity by using the spatial interpolating. For further details of the procedure, the reader should refer Kojima and Suzuki (2005). (5) the thickness of the alluvium and diluvium are calculated from the observed predominant periods and the averaged S-wave velocities by using the quarter-wavelength rule.

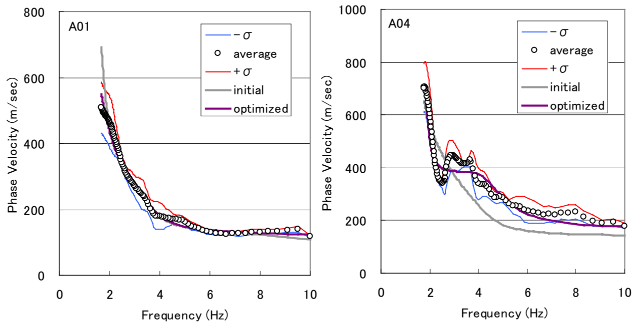

Figure 6. Comparison between observed and theoretical dispersion curves

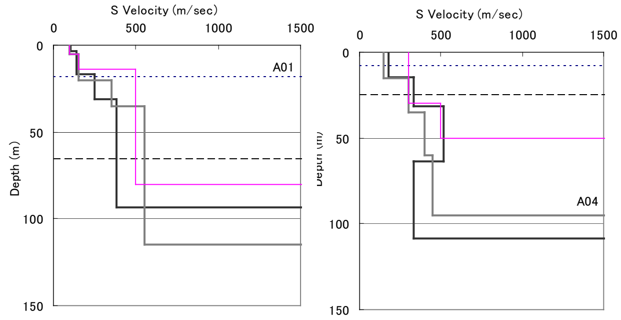

Figure 7. Comparison of optimized S-wave velocity structure (black line) with initial structure (gray line).

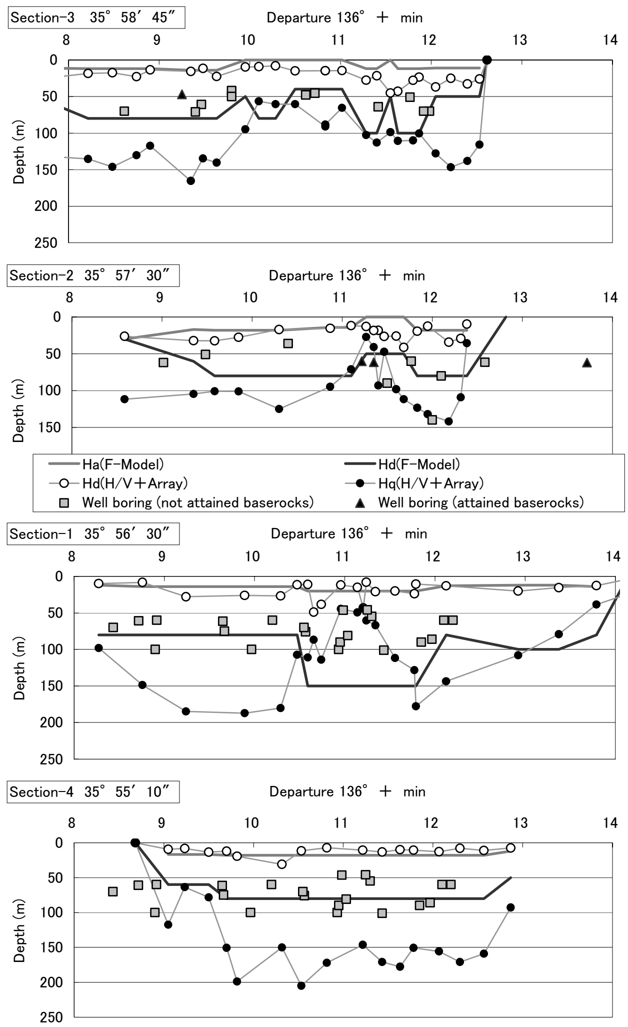

Figure 8. Subsurface cross sections along the four exploration lines.

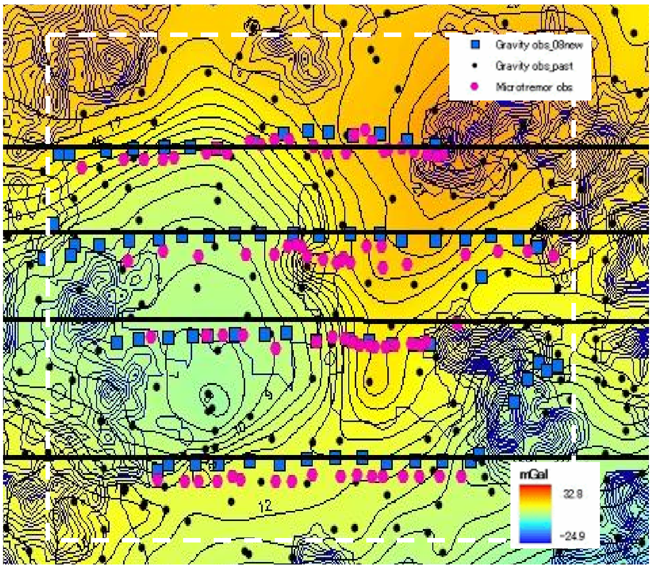

Figure 9. Contour map of the residual Bouguer gravity anomaly

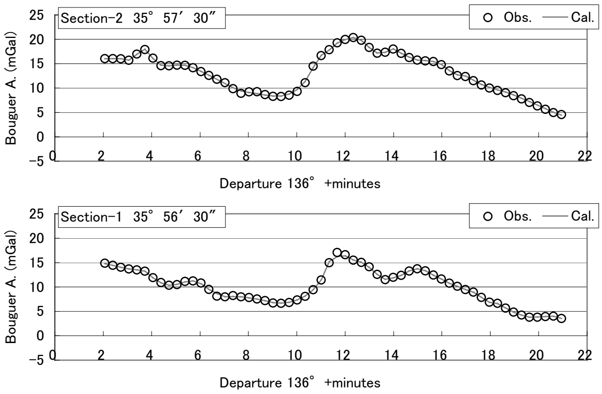

Figure 10. Comparison of the observed Bouguer anomaly and the calculated anomaly for the estimated structure

The open circles in Figure 8 show the distribution of the estimated depths of the alluvial layer along the exploration lines whereas the filled circles exhibit those of the quaternary deposit. It can be observed that the thickness of the quaternary tends to increase toward the center of the basin except for the Sabae Plateau area from the edge. There are abrupt discontinuities of the Quaternary deposit near the Sabae Fault in the section-1 and 2. The Tertiary baserock seems to be shifted over 100m across the fault at these sections. However, the other two sections have only obscure offsets and gradual inclinations of the layers.

The gray and black lines in the figure represent the Quaternary configurations of the F-model. It seems to be not consistent with the topographic aspect that the F-model has a deep depression beneath the plateau in the section 2. The gray squares show the depths of existing deep wells suspended in the Diluvium and the gray triangles exhibit those attained the Tertiary bedrock. It is confirmed that the estimated Quaternary depths are lower than almost all the suspended well. The F-model's Quaternary depth seems to be too shallow considering that several suspended wells are deeper than its depth.

4.3 Density Structure

Dots in Figure 9 indicate the observation points contained in the gravity CD-ROM of Japan (Ver.2) published by the Geological Survey of Japan. We carried out an additional gravity observation along the four sections by using a Racoste Lon Berg's G type gravimeter. Those about 70

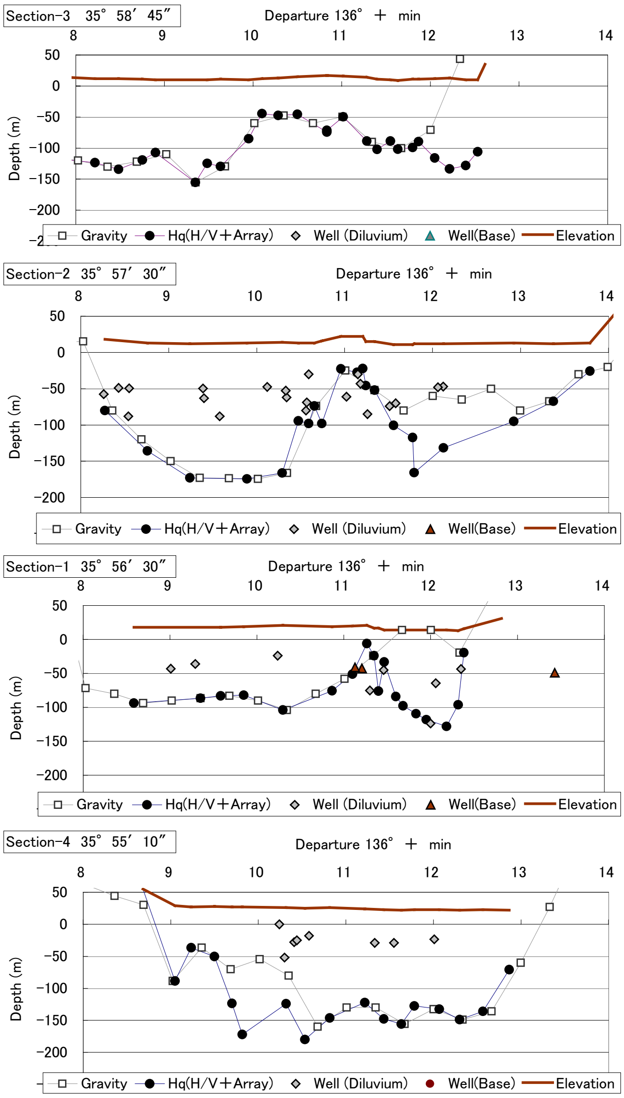

Figure 11. Comparison of the Quaternary configuration

observation points are shown by squares in Figure 10. Kobayashi et al. (2001) calculated 3D density structure beneath the Fukui plain (northern than 36 degree N) up to a depth of 4 km by applying 2D-Talwani's method. They used a three-layer model; i.e., from top to bottom, each layer corresponds to the Quaternary sediments (density 2.1g/cm3), the Neogene sedimentary layers (2.4), and the lowest Neogene layer and the lower strata (2.67), respectively. By considering the continuity of the geological condition around the Fukui plain, we judged those three layers system was able to adopt in the Seibu basin. To remove the deep structure effect, a band pass filter was used that combines two upward continuation filters of 50 and 1000m. The terrain correlation was made with a topographic 50m- and 250m-mesh digital data to obtain the Bouguer gravity anomaly. The contour map of residual Bouguer gravity anomaly is shown in Figure 9. The eastern low land shows relatively high gravity anomaly, while the western low land has lower anomaly.

We estimated the 2D density structure of the exploration section based on the Bouguer anomaly by restricting the depths of the bedrock layer to the outcrop points in the mountainous area. Figure 10 indicates observed anomalies (open circles) and theoretical anomalies (solid line) for the estimated density structure. It is confirmed that the estimated structure could reproduce the observed anomaly with sufficient accuracy. Figure 11 compares the density

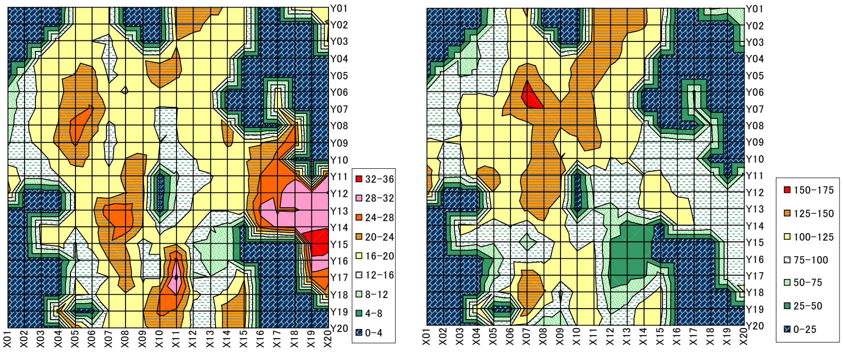

Figure 12 Contour maps of the depth of Alluvium(left) and Quaternary(right)

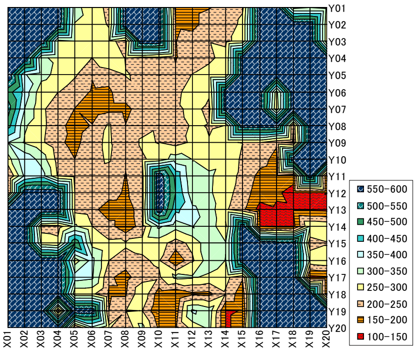

Figure 13 Contour map of Vs30

structure (the boundary between the Quaternary and the Neogene layer) with the estimated configuration from the microtremor observations. In the west lowland area, the density structures show fairly good agreement with the estimated Quaternary configurations. However, in the east lowland, the density structures were estimated too shallow. It is considered that the cause of such results seems to be in the hypothesis where the 3-layers model is evenly accepted in horizontal direction (see Figure 9).

4.4 3D Configuration

The 3D S-wave velocity structure was estimated based on the inverted and the interpolated vertical S-wave velocity structure of the microtremor observation sites. The area of estimation is corresponding to the 1/25,000 topographic map of Sabae published by the Geographical Survey Institute. The latitude and longitude of the south-west edge are 35° 55' and 136° 7.5', and the ones of the north-east are 36° and 136° 15', respectively. The estimation was carried out on the center of every square mesh of 0.375 by 0.25 minute in longitudinal and latitudinal direction. The 3D configuration models of Quaternary have been evaluated by using a spatial interpolation. The thickness and S-wave velocity of each layer of the mesh were calculated as the weighted mean value of the nearest several microtremor observation points. The weight was assumed to be inverse proportion to the square of distance. The thicknesses of Alluvium and Quaternary layers were determined as illustrated in Figure 12. Figure 13 represents the distribution of the Vs_{30} (averaged S-wave velocity up to –30m). The estimated configuration shows that the Tertiary bedrock has a folded mound along the Sabae Fault and that the deep Quaternary depressions are distributed along the Hino River bed. However, the estimated 3D configuration seems to be too complicated to explain by a simple normal or reverse fault movement.

5 CONCLUSION

The quaternary configuration around the Seibu Basin was estimated by using the microtremor observation data. The array and the single point 3-components microtremor observations were conducted along the several exploration lines orthogonal to the Sabae Fault. The dispersion curves at each array site were inverted to a vertical S-wave profile using a genetic algorithm. To interpolate the array observations, we estimated the quaternary configuration from the predominant periods of H/V spectrum using the estimated S-wave velocities based on the quarter wavelength rule. The validity of the estimated structure was confirmed by comparing with the inverted structure of gravity anomaly observation and with the existing deep well data. The estimated underground configuration seems to suggest that the Sabae Plateau formed by the continuous activity of the Sabae Fault. However, there have been no seismic exploration surveys around the Sabae Fault. We expect the Japanese government to execute a number of conclusive explorations, deep borings or seismic explorations, to improve the accuracy and reliability of the quaternary model.

REFERENCES

Fukui Prefecture, 1997, Report of earthquake disaster prediction investigation in Fukui Prefecture.

Geological survey of Japan (AIST), 2004, Gravity CD-ROM of Japan, Ver.2.

Kitsunezaki, C., Goto, N., Kobayashi, Y., Ikawa, T., Horike, M., Saito, T., Kurota, T., Yamane, K. and Okumizu, K. 1990. Estimation of P- and S-wave velocities in deep soil deposits for evaluating ground vibrations in earthquake, Jour. Natural Disaster Science, 9; 3; 1-17 (in Japanese).

Kobayashi, N., Hiramatsu, Y., Kono, Y. and Takeychi, F. 2001, 3D basement structure of the Fukui plain, central Japan, inferred from gravity anomalies, Jour. of Seis. S. of Japan, Vol.54, No.1, 1-8, (in Japanese).

Kojima, K. and Yamanaka, H. 2004, Estimation of Quaternary structure of the Fukui plain based on microtremor observation, Proc. of JSCE, No.752/I-66, 217-225, (in Japanese).

Kojima, K. and Suzuki, D. 2005, Estimation of Quaternary configuration of Fukui plain based on Geostatistical method and microtremor observation, Jour. Japan Soc. Eng. Geol. Vol.46, No.1, 9-19, (in Japanese).

Kojima, K., Tsujimori, T. and Nouka, K. 2004, Estimation of S-wave velocity structure of east-west cross section of the Fukui plain based on microtremor observation, Jour. of Applied Mechanics JSCE, Vol.7, 119-128, (in Japanese).

National Astronomical Observatory, 1994, Chronological Scientific Tables, 822-853.

Noguchi, T. and Nishida R. 2002, Determination of subsurface structure of Tottori plain using microtremors and gravity anomaly, Jour. of Natural Disaster Science, Vol.24, No.1, 1-13.

Komazawa, M. 1995, Gravimetric analysis of volcano and its interpretation, Jour. Geod. Soc. Japan, Vol.41, No.1, 17-45.

Nagao, T. and Konno, K. 2001. Estimation of average S-wave velocity of ground by use of microtremor array observation, Proc. of JSCE, No.696/I-58, 225-235, (in Japanese).

Yamamoto, H., Okamoto, T., Kojima, K. Kinoshita, K. and Edo, S. 2008, Geographical feature and trench survey of the Sabae faault in the Seibu basin, Fukui orefecture, Vol.30, No.10, 489-496, (in Japanese).